Comparative analysis of nanometric inspection methods in fringeless speckle pattern interferometry

PABLO ETCHEPAREBORDA[1,*], ANA LAURA VADNJAL[1], ARTURO BIANCHETTI[2], FRANCISCO E. VEIRAS[3], ALEJANDRO FEDERICO[2], AND GUILLERMO H. KAUFMANN[4]

[1]*Electrónica e Informática, Instituto Nacional de Tecnología Industrial, CONICET, P.O. Box B1650WAB, B1650KNA San Martín, Argentina*
[2]*Electrónica e Informática, Instituto Nacional de Tecnología Industrial, P.O. Box B1650WAB, B1650KNA San Martín, Argentina*
[3]*Laboratorio de Sistemas Líquidos, GLOmAe, Departamento de Física, Facultad de Ingeniería, Universidad de Buenos Aires, Avenida Paseo Colón 850, Ciudad Autónoma de Buenos Aires, C1063ACV, Argentina*
[4]*Instituto de Física Rosario, Ocampo y Esmeralda, S2000EZP Rosario, Argentina*
[*]*Corresponding author: pabloe@inti.gov.ar*

Compiled October 7, 2016

The application of a straightforward arccosine function to a filtered interferogram, the Correlation of Images (CoI) and the Implicit Smoothing Splines (ISS) are analyzed and compared for fast inspection of nanometric displacement fields avoiding the acquisition of several images. The arccosine and the CoI approaches are also used as seed solution for the ISS method and the performance of the recovered phase is evaluated by means of numerical simulations. Three different methods for the normalization of fringeless speckle interferograms are proposed and compared. A summary of conclusions is given as an orientation to the analysis of fringeless speckle interferograms.

OCIS codes: *(100.0100) Image processing; (100.2000) Digital image processing; (100.5070) Phase retrieval; (120.4630) Optical inspection; (120.6160) Speckle interferometry.*

http://dx.doi.org/10.1364/ao.XX.XXXXXX

1. INTRODUCTION

In the last two decades, non-invasive measurements of mechanical deformation have received great attention in the microsystems industry due to the need of feedback about device behavior, system parameters, and material properties [1–4]. As mechanical properties of bulk materials cannot be scaled down to micron-sized systems, the development and quality control of miniaturized components in micro-sensors and Micro-(Opto-)Electro-Mechanical Systems [M(O)EMS] require dedicated, low-cost, fast and reliable testing methods. Moreover, full field testing methods are needed to reduce dynamical and dimensional restrictions of the measurements of specimens with nonhomogeneous states. Consequently, different alternatives based on frameworks that pushes complexity to the numerical processing stage must be explored.

In M(O)EMS, dimensional measurements are mainly carried out by optical non-contact methods, including the performance testing of dynamic final devices [5]. Speckle interferometry techniques have been widely used for full-field displacement measurements due to their sensitivity and adaptable experimental arrangement [6]. The interferometric approach is based on the evaluation of the optical phase changes that are coded in speckle interferograms recorded by a spatial light sensor for different states of the specimen. The phase changes are associated to a displacement field at the rough surface of the specimen according to a sensitivity direction given by the optical setup.

Phase shifting interferometry (PSI) techniques are common methods for decoding the optical phase changes [7], which need a precise control of a piezoelectric or electro-optical actuator to modify the optical phase of the reference or the object beam in order to acquire several different interferograms for an initial state of the sample and the deformed state. The algorithms used for calculating the phase maps are based on either phase of differences method (PDM) or difference of phases method (DPM) [8]. In the PDM, the phase map due to displacements is obtained by analyzing phase shifted correlation fringe patterns, whereas in DPM, the phase change is calculated by subtracting the phase data obtained from the initial state images and other phase data obtained from the deformed state images. The displacement field is finally determined by processing the phase map with a phase unwrapping technique. Besides the experimental complexity involved in PSI, all algorithms assume that the object remains invariant during phase shifts. Therefore, the optical setup and environmental conditions must be well controlled in order to obtain the expected accuracy. In contrast to PSI, single frame analysis techniques enables dynamic measurements and achieve high robustness to

environmental disturbances [9]. Then, they are suitable for out-of-laboratory measurements. In Digital Speckle Pattern Interferometry (DSPI), only a first image corresponding to the initial state of the sample and a second image of the deformed state are acquired. The subtraction of these images produce a new one with an emerging fringe pattern related with the displacement field of the specimen under test.

The Implicit Smoothing Splines (ISS) method is capable of extracting the continuous phase distribution from DSPI fringe patterns showing high versatility with respect to spatial fringe density [10]. The method uses piecewise polynomial functions for fitting a smooth phase change distribution that would generate the DSPI data with limited global admissible error. This approach requires to resolve an optimization problem in the form of a nonlinear system of equations depending on the normalized data values. The global character of the ISS model makes the solution highly dependent of an initial phase guess that must be provided to the numerical solver. Under proper initial phase guess, the method estimates the continuous phase distribution without ambiguity and no phase unwrapping procedure must be applied. Moreover, a limited number of non-critical parameters need to be specified and does not require the supervision of an external operator.

Nowadays, more sensitive methods are developed to characterize fields of nanometric displacements in the inspection of M(O)EMS devices, nanopositioning systems and sensors for micromanipulators [11]. In these situations, the optical phase change does not surpass the 2π limit and no fringes are produced. The absence of fringes in the speckle interferogram difficults the application of fringe pattern processing methods based on automatic normalization and phase extraction [12–21] for automatic fringe analysis processing. A technique that enables phase recovery in fringeless interferograms is based on speckle correlation patterns generated by calculating the local correlation coefficient between two DSPI patterns [22, 23]. This approach, addressed in this work as the Correlation of Images method (CoI), does not require uniform illumination over the surface of the object neither the application of a spatial phase unwrapping procedure to obtain the continuous phase distribution.

In this work, we analyze the performance of different single frame phase recovery and normalization methods to be applied to fringeless DSPI. We tested three normalization procedures: (1) acquisition of single beam images (SBI), (2) phase guess based normalization using spline interpolation (PGS) of a filtered DSPI fringeless pattern (DSPI-FP), and (3) phase guess based normalization using least squares fitting of single interferograms to DSPI-FP. To retrieve the phase map, we used three different methods for the DSPI pattern: (1) arccos of DSPI-FP, (2) Correlation of Images, and (3) ISS (with CoI or arccos initial phase guess). We evaluate the performance of these methods by using speckle images simulated at different conditions and also applied these methods to an excited piezoelectric device. Finally, we give a summary of conclusions as an orientation for the analysis of fringeless images in DSPI for the inspection of nanometric displacement fields.

2. ANALYSIS OF FRINGELESS SPECKLE INTERFEROGRAMS

In out-of-plane speckle interferometry, the recorded intensity can be modeled by the two-beam interferometric equation

$$I_a = I_{aB} + I_{aM}\cos(\phi_s), \tag{1}$$

where spatial coordinates (m,n) were omitted for clarity and the subscript a denotes the initial state of the specimen. I_{aB} is the bias intensity given by the sum of the illumination intensities of the reference and object beams, I_{aR} and I_{aO}, respectively. I_{aM} is the modulation intensity that affects the cosine term which phase is determined by the random speckle phase ϕ_s, uniformly distributed over $[-\pi,\pi)$ rad [24]. The modulation intensity depends on the illumination intensities of the two beams by the relation $I_{aM} = 2\sqrt{I_{aR}I_{aO}}$.

When a second image is obtained for a deformed state of the sample (subscript b), the intensity assumes values according to

$$I_b = I_{bB} + I_{bM}\cos(\phi_s + \Delta\phi), \tag{2}$$

where $\Delta\phi$ accounts for the phase change introduced by the field of displacement d of the surface of the object depending on the laser wavelength λ as $\Delta\phi = 4\pi d/\lambda$.

Assuming the approximation $I_{aR} = I_{bR} = I_R$, $I_{aO} = I_{bO} = I_O$, and defining $I_{aM} = I_{bM} = I_M$ and $I_{aB} = I_{bB} = I_B$, the correlation speckle fringe patterns $\Delta I \equiv (I_a - I_b)^2$ can be written in the form

$$\Delta I = 8 I_R I_O \sin^2\phi_s\,(1-\cos\Delta\phi). \tag{3}$$

It worth noting that, for sufficiently smooth $\Delta\phi$, a spatial average of ΔI can be written as

$$\overline{\Delta I} \approx 4\bar{I}_R\bar{I}_O(1-\cos\Delta\phi). \tag{4}$$

In the following two subsections, we present three different phase recovery methods and three normalization techniques that will be considered for the analysis of fringeless speckle patterns ΔI.

A. Phase recovery methods

A.1. Arccosine of DSPI-FP

A straightforward way of processing a normalized DSPI-FP is the use of the arccos function (inverse cosine) [25]. A number of methods of different complexity for optimizing the SNR in speckled fringe patterns has been reported in the bibliography [26]. The normalized and filtered image takes values $0 \le \overline{\Delta I}_n \le 2$ and the phase can be estimated by the expression

$$\widehat{\Delta\phi} = \arccos(1-\overline{\Delta I}_n), \tag{5}$$

where Eq. (4) was used.

A.2. Correlation of images

In the condition of fully developed and polarized speckle, the phase and intensity fields become statistically independent and the phase change $\Delta\phi$ is related with the Pearson's correlation coefficient between images I_a and I_b by the equation

$$C_P(I_a - I_{aB}, I_b - I_{bB}) = \frac{\langle I_{aM} I_{bM}\rangle}{\sqrt{\langle I_{aM}^2\rangle\langle I_{bM}^2\rangle}}\cos\Delta\phi, \tag{6}$$

where C_P the Pearson's correlation coefficient between the two interferograms and the operator $\langle\rangle$ is evaluated over a sliding window of size $L\times L$ on each recorded image [27]. The introduction of two approximations overcomes limitations of applicability and achieve higher accuracy [23]: (1) the influence of the intensity bias in the correlation coefficient can be ignored, (2) the modulation term in Eq. (6) can be assumed equal to 1. In addition, the Pearson's coefficient is replaced by the Order Statistics Correlation Coefficient C_{OS} that possesses high sensitivity to changes in association, superior noise robustness, small

biased and fast computational speed [28]. Therefore, Eq. (6) can be reformulated as

$$\widetilde{\Delta\phi} = \arccos[C_{OS}(I_a, I_b)], \tag{7}$$

where $\widetilde{\Delta\phi}$ is the estimated phase change introduced by the deformation. The pixel by pixel computation of $C_{OS}(I_a, I_b)$ implies the use of a moving sliding window of size $L \times L$.

A.3. Implicit Smoothing Spline

The Implicit Smoothing Spline (ISS) method allows to define the smoothing spline approximation $S(x)$ of a distribution when the provided noisy input data Y_i represents some known function f of $S(x)$ at particular knots x_i with integers $1 \leq i \leq N$ [10]. The cubic spline is considered in this work motivated by its strain energy minimization property and simple framework [29]. A smoothing spline achieves a balance of smoothness and interpolation error by means of the adjustment of a single parameter p in the penalized sum of squares functional

$$P_f(S) = \sum_{i=0}^{N} [Y_i - f(S_i)]^2 + p \int_\Omega [S''(x)]^2 dx, \tag{8}$$

where $S_i = S(x_i)$ with the spline function $S(x)$ evaluated at the knots x_i corresponding to each pixel in the interpolation domain Ω. In Eq. (8), the first term is related to the interpolation error of $S(x)$ against data and the second one is the second derivative of $S(x)$. The minimization of $P_f(S)$ is carried out by solving the system of equations

$$f'(\hat{\mathbf{S}}) \cdot [\mathbf{Y} - f(\hat{\mathbf{S}})] = pK\hat{\mathbf{S}}, \tag{9}$$

where we denoted elementwise multiplication by the central dot symbol and f' represents the analytical differentiation of f. The vectors $\mathbf{Y}$ and $\hat{\mathbf{S}}$ contain the values of input data and the solution at the interpolation knots, Y_i and S_i. K is an $N \times N$ matrix of constant coefficients that, in the cubic spline case and being x_i the location of consecutive pixels in a row (or column), presents the sparse form $K = Q^T G^{-1} Q$ with

$$\begin{aligned} &G_{ii} = 2, \qquad G_{i-1,i} = G_{i,i-1} = 0.5, \\ &Q_{ii} = 1, \qquad Q_{i,i+1} = -2, \qquad Q_{i,i+2} = 1, \end{aligned} \tag{10}$$

where G is a matrix of size $(N-2) \times (N-2)$ and Q has size $(N-2) \times N$. The choice of p allows to obtain: (1) a direct spline interpolation ($p = 0$), (2) a straight line least squares fit ($p \to \infty$), and (3) the whole spectrum of smoothed solutions in between.

From Eq. (3), the function of phase $f(\Delta\phi) = 1 - \cos(\Delta\phi)$ is used to estimate $\widetilde{\Delta\phi}$. According to Eq. (9), this choice of f leads to the nonlinear system of equations with the unknown vector $\hat{S}$

$$\sin(2\hat{\mathbf{S}}) - 2(1 - \mathbf{Y}) \cdot \sin(\hat{\mathbf{S}}) = 2pK\hat{\mathbf{S}}. \tag{11}$$

As the function f is continuous and smooth, any gradient-based nonlinear algebraic solver is expected to perform well. We recommend the use of a trust-region Powell dogleg method for which the Jacobian matrix should also be provided [30]. We want to emphasize that, as the periodicity of f induces solution branches mutually shifted by $2k\pi$ (k integer), the initial condition for the nonlinear solver has to be carefully chosen. Note that ISS solves the optimization problem using just one unknown variable (e.g. phase value) for each knot.

In Ref. [10], a complete algorithm was presented to apply the ISS method in phase decoding of fringe patterns by using skeletonization and Thin Plate Spline interpolation to obtain an initial phase guess. A one-dimensional ISS solver was applied for every row and column of the interferogram arriving at two corresponding different solutions that can be averaged and smoothed with 2D cubic splines to complete the phase estimation. The normalization preprocessing is performed to transform the data obeying Eq. (3) by adopting

$$Y \approx \frac{2I_M}{\overline{I_M}} \sin^2(\phi_s)[1 - \cos(\Delta\Phi)]. \tag{12}$$

Note that the arccos and CoI methods can be integrated to ISS as they provide fine approximations to the optical phase field which is introduced as seed solution to the nonlinear solver. In the following subsection, we show other ways to integrate phase recovery methods during the normalization step.

B. Normalization methods

The speckle modulation produced by the phase change can be easily confused with effects generated by uneven illumination. Therefore, a robust normalization method is required to obtain a good performance in the phase recovery processing. Below we present three methods of normalization in order to test the performance of the three phase recovery techniques.

B.1. Single beam images (SBI)

The images corresponding to the intensity of the reference I_R and object I_O beams are acquired separately. These two images are spatially filtered and considered to normalize the DSPI-FP described by Eq. (4) as $\Delta I_{n1} = \Delta I / (4\bar{I}_R \bar{I}_O)$. This method allows to apply either the arccos, CoI or ISS methods directly. It is worth noting that the seed solution for ISS should be similar to the actual phase map as the one obtained by the arccos or CoI methods.

B.2. Phase guess based normalization using spline interpolation (PGS)

The CoI method does not require an initial normalization process for obtaining a phase guess solution ϕ_G that may be used for normalizing ΔI without the need of acquiring extra images. ϕ_G is used as an initial phase guess to model the DSPI-FP for the approximation $\overline{\Delta I} \approx I_S(1 - \cos\phi_G) = I_S f_G$, where I_S is a 2D spline surface and $f_G = (1 - \cos\phi_G)$. The interpolating 2D spline can be obtained by averaging the results from row-wise and column-wise analysis where each row or column solution is found by solving a linear system of equations given by

$$(2\mathbf{f_G}^2 I_{\mathbf{N}} + \rho K)\mathbf{I_S} = 2\overline{\mathbf{\Delta I}} \cdot \mathbf{f_G}, \tag{13}$$

where $I_{\mathbf{N}}$ is the N dimensional identity matrix, $\mathbf{f_G}^2$, $\mathbf{I_S}$ and $\overline{\mathbf{\Delta I}}$ are vectors containing all the elements in one row or column of f_G^2, I_S and $\overline{\Delta I}$, respectively. ρ is a smoothness parameter and K is the cubic spline matrix as described in Eq. (10). Finally, $\Delta I_{n2} = \Delta I / I_S$.

B.3. Phase guess based normalization using least squares fitting (PGLS)

In this phase guess based normalization method, we use the filtered interferograms $\bar{I}_a$ and $\bar{I}_b$ and consider the use of the illumination intensity $I_i = (\bar{I}_a + \bar{I}_b)/2$. If the reference beam is homogeneous in amplitude, then the modulation intensity in Eq. (4) can be found by an affine transformation of I_i, $\overline{I_M^2} \approx \alpha I_i + \beta$. Considering Eqs. (1-2) and $I_R = R$, then $I_i \approx R + \bar{I}_O$ and the coefficients should be $\alpha = 4R$ and $\beta = -4R^2$. In this work, we obtain α and β as the best fit of our model to ΔI in

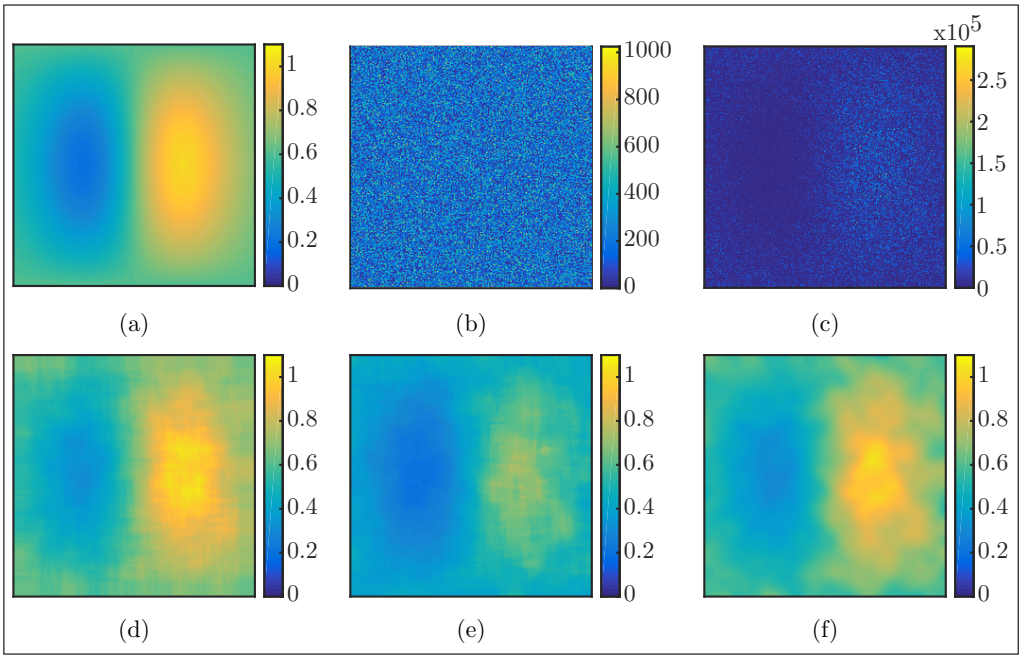

Fig. 1. (a) Original phase distribution obtained by simulation ($\Delta\phi_0$ in radians), (b) initial state interferogram, (c) fringeless pattern given by the square difference between interferograms of initial and deformed states (DSPI-FP). Phase maps in radians recovered by (d) CoI method, (e) arccos method with SBI normalization, and (f) ISS method with PBLS normalization.

a least-squares sense. The obtained overdetermined system of linear equations is expressed by

$$\begin{bmatrix} \mathbf{I}_i \cdot \mathbf{f}_G & \mathbf{f}_G \end{bmatrix} \begin{bmatrix} \alpha \\ \beta \end{bmatrix} = \mathbf{\Delta I}, \tag{14}$$

where the coefficients are calculated by a matrix inversion and the normalization of the DSPI-FP is performed as $\Delta I_{n3} = \Delta I / (\alpha I_i + \beta)$.

3. NUMERICAL TESTS

We analyzed the performance of the normalization and phase recovery methods for several conditions of SNR, illumination homogeneity, mean speckle grain size, phase excursion and smoothness parameters. All the synthetic speckle interferograms were generated using a commonly adopted method based on a $4f$ optical system [31]. The simulated speckle images of an out-of-plane interferometer were obtained as the intensity of a complex amplitude described by the usual Gaussian first-order speckle statistics. According to this model, the intensity can be simulated as

$$I = |A_R + \mathcal{F}^{-1}\{H\mathcal{F}[A_O \exp(i\theta)]\}|^2, \tag{15}$$

where A_O sets the amplitude distribution of the simulated object beam, A_R is the amplitude of the reference beam, i is the imaginary unit, $\theta = \phi_s$ for the initial state interferogram and $\theta = \phi_s + \Delta\phi$ for the deformed state image. $\mathcal{F}$ and $\mathcal{F}^{-1}$ denote the direct and inverse 2D fast Fourier transform, respectively. H acts as a circular low pass filter with radius $a \leq N/2$, which sets the average speckle size $s_o = N/(2a)$.

The images were simulated for a size 256×256 pixels in a scale of 10-bit gray levels with $s_o = 1.1$ pixel. Additive Gaussian noise η_G with a variance σ_G^2 was incorporated to the intensity model as $I_G = I + \eta_G$. The images contanining the expected SNR were obtained by taking $\sigma_G^2 = \sigma_I^2 10^{-\mathrm{SNR}/10}$, being σ_I^2 the variance of I.

The normalization and phase recovery methods were applied to the simulated speckle interferograms in order to assess their performance under different conditions. The quality Q of the recovered phase map was evaluated with the structural similarity (SSIM) index [32]. The distortion measured by the SSIM index is associated to loss of correlation, undesired offset of the mean phase, or modification of the standard deviation. $Q \in [-1, 1]$ and $Q = 1$ is satisfied for exact phase recovery. Q was calculated as the mean value of several Q_j of locally obtained SSIM indices using a sliding window approach and considering the relation

$$Q_j = \frac{(2\overline{\phi}_A\overline{\phi}_B + C_1)(2\sigma_{\phi_A\phi_B} + C_2)}{(\overline{\phi}_A^2 + \overline{\phi}_B^2 + C_1)(\sigma_{\phi_A}^2 + \sigma_{\phi_B}^2 + C_2)}, \tag{16}$$

where ϕ_A and ϕ_B are the images being compared, $\overline{\phi}$ is the mean value of ϕ, σ is the standard deviation and $\sigma_{\phi_A\phi_B}$ is the correlation coefficient between ϕ_A and ϕ_B. C_1 and C_2 are small positive constants that avoid numerical instability for near zero sample means, standard deviations or correlation coefficients. $C_1 = 0.002$ and $C_2 = 0.006$ were chosen to obtain comparable results.

A. Homogeneous illumination

The first set of simulations was used to analyze the most straightforward situation of homogeneous illumination and object and reference beams with equal intensities. For this purpose, we used the displacement field which generated the phase change $\Delta\phi_0$ shown in Fig. 1(a). A multiplicative factor A_ϕ was introduced in the simulations to obtain a phase change with maximum value equal to A_ϕ, $\Delta\phi = A_\phi\Delta\phi_0$.

In Fig. 1(b) we show the speckle interferogram obtained for R such that I_R is 2 times higher than $\overline{I}_O$ and considering a low

Table 1. SSIM index for the CoI, arccos **and ISS phase recovery methods with the normalization SBI and PGLS obtained for different SNR and A_ϕ with homogeneous illumination in both beams.**

SNR	A_ϕ [rad]	CoI	arccos		ISS	
			SBI	PGLS	SBI	PGLS
10 dB	0.2	0.76	0.91	0.91	**0.99**	0.91
	1	0.97	0.98	0.98	0.97	**0.99**
	2.5	**0.99**	0.93	0.93	0.97	**0.99**
6 dB	0.2	0.58	0.81	0.79	**0.95**	0.79
	1	0.92	0.97	**0.98**	0.96	**0.98**
	2.5	**0.99**	0.90	0.91	0.94	**0.99**

noise situation ($SNR = 15$ dB), where the homogeneity of illumination can be observed. Fig. 1(c) corresponds to a DSPI-FP with $A_\phi = 1$ rad, where the mean intensity of the speckle grains presents spatial variations. The phase map recovered by the CoI method ($L = 25$) is shown in Fig. 1(d) for a SSIM index of $Q = 0.994$. The next two images correspond to the phase maps recovered by the (e) arccos method when the SBI normalization was used ($Q = 0.975$) and (f) the ISS method ($p = 1$) with PGLS normalization ($Q = 0.997$). Note that the solution given by the ISS is smoother than the CoI result. The nonlinear equation solver in the ISS method was implemented with 12 iterations. The processing time of the ISS method was 4 times slower than the CoI technique and 63 times slower than the arccos approach. Three significant numbers were required to compare the obtained SSIM indices for this low noise situation. The following simulations were performed with lower levels of SNR.

Table 1 presents the SSIM index obtained for different SNR, A_ϕ values and phase recovery methods, using the intensity of the reference beam $I_R = 2\bar{I}_O$. The size of the sliding window in the CoI and the arccos methods (L), and the smoothness parameter of the ISS technique (p) were corrected for each situation in order to maximize the resulting SSIM indices. We suggest the use of $L \approx 25$ and an initial $p \approx 1$, which can be reduced down to $p = 0.001$ if a low phase excursion is detected, or it can be incremented to $p = 10$ otherwise. Further details on the configuration of the smoothness parameter are described in subsection C. As a first observation, it is seen that a most notorious decay of performance given by a drop in the SNR is produced at low phase excursion situations. In this table, the best SSIM index for every case is highlighted in bold. It is also observed that the arccos method produces a better performance at medium values of phase excursions. We emphasize the performance given by the ISS-PGLS combination, even in comparison with the ISS-SBI approach, which requires the acquisition of two more images. The stability of the performance against increased noise or varying phase excursions is another advantage we observe for the ISS method.

B. Uneven illumination

Two different sets of simulated images were analyzed for the cases of (a) uneven illumination in both beams and (b) an inhomogeneous object beam. In these situations, the DSPI-FP normalization process has a key role in determining which changes

Table 2. SSIM index for the CoI, arccos **and ISS phase recovery methods with the normalization SBI, PGS and PGLS obtained for different A_ϕ with an uneven illumination in both beams and for SNR values of (a) 10 dB and (b) 6 dB.**

(a) SNR = 10 dB

A_ϕ [rad]	CoI	arccos			ISS		
		SBI	PGS	PGLS	SBI	PGS	PGLS
0.2	0.71	0.85	0.84	0.84	**0.96**	0.84	0.84
1	0.96	**0.98**	0.97	0.96	0.96	**0.98**	**0.98**
2.5	**0.99**	0.91	0.90	0.85	0.93	**0.99**	0.96

(b) SNR = 6 dB

A_ϕ [rad]	CoI	arccos			ISS		
		SBI	PGS	PGLS	SBI	PGS	PGLS
0.2	0.55	0.77	0.72	0.72	**0.93**	0.71	0.71
1	0.90	**0.97**	0.96	0.96	0.96	0.96	0.96
2.5	**0.99**	0.87	0.89	0.86	0.87	**0.99**	0.97

in the speckle modulation correspond to illumination variations and which depend on the phase changes generated by the sample. In the simulations, we used intensities presenting Gaussian shaped illumination spots with a center located at $\mu_O = [-16, 0]$ px, being $o = [0, 0]$ px the center of the image, and a full width at half maximum $\text{FWHM}_O = 270$ px for the object beam. We also used $\mu_R = [0, 0]$ px and $\text{FWHM}_R = 330$ px for the reference beam. The intensities of the reference and object beams are shown in Figs. 2(a) and 2(b), respectively. The filtered subimage allows to observe the inhomogeneity presented by the object beam. Fig. 2(c) shows effects of an uneven illumination in the image acquired in the initial state of the sample. The DSPI-FP shown in Fig. 2(d) is affected by the inhomogeneity of the interfering beams. The normalized DSPI-FP obtained by the SBI method is shown in Fig. 2(e), with values mainly between 0 and 2. The following three images shown in Fig. 2 correspond to the recovered phase maps given by (f) the CoI method ($L = 25$), (g) the arccos technique with the SBI normalization and (h) the ISS approach ($p = 1$) with the PBLS normalization. It is observed that the phase field recovered by the ISS method is closely related to the original phase map shown in Fig. 1(a), except at the corners where the illumination intensity of the reference beam have minimum values and the phase is underestimated. On the other hand, the CoI method overestimates the phase values at the corners of the image and arccos technique with the SBI normalization gives a correct recovered phase at the corners but the phase is underestimated at the regions presenting the highest phase excursion.

As in the previous subsection, similar simulations were performed for these uneven illumination situations and the obtained SSIM indices are presented in Tables 2 and 3. In these cases, we have added the results given by the PGS normalization method in order to assess its performance when the arccos and ISS techniques were applied. As before, in every SNR-A_ϕ situation, the best performance is highlighted in bold. We want to remark the convenience of using the SBI normalization for

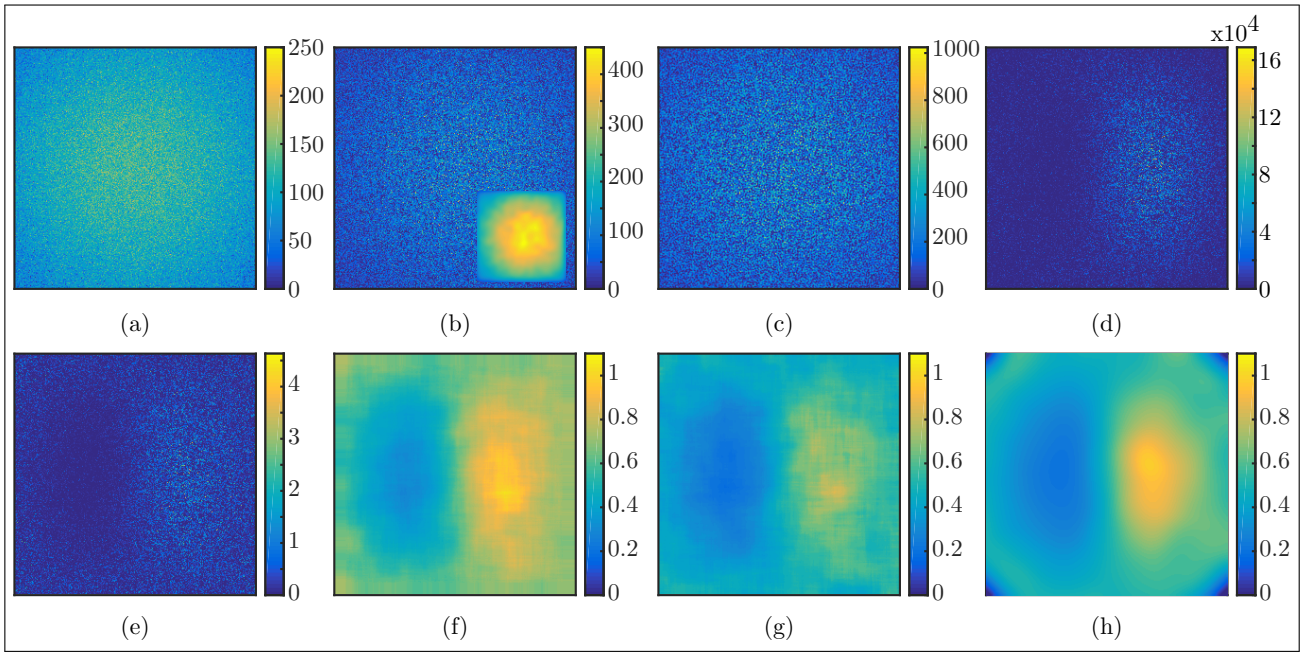

Fig. 2. (a) Simulated acquisition of a non interferometric image where the object beam is obstructed (I_R), (b) image acquired with an obstructed reference beam (I_O) and the low-pass filtered subimage, (c) single interferogram for the initial state, (d) DSPI-FP, (e) normalized DSPI-FP using the SBI approach. Phase maps in radians recovered by (f) the CoI method, (g) the arccos technique with the SBI normalization, and (h) ISS approach with the PBLS normalization.

Table 3. SSIM index for the CoI, arccos **and ISS phase recovery methods with the normalization SBI, PGS and PGLS obtained for different A_ϕ with uneven illumination in the object beam and for SNR values of (a) 10 dB and (b) 6 dB.**

(a) SNR = 10 dB

A_ϕ [rad]	CoI	arccos			ISS		
		SBI	PGS	PGLS	SBI	PGS	PGLS
0.2	0.75	0.89	0.87	0.88	**0.98**	0.88	0.88
1	0.97	0.98	0.98	0.97	0.97	**0.99**	**0.99**
2.5	**0.99**	0.92	0.93	0.93	0.96	**0.99**	**0.99**

(b) SNR = 6 dB

A_ϕ [rad]	CoI	arccos			ISS		
		SBI	PGS	PGLS	SBI	PGS	PGLS
0.2	0.58	0.80	0.76	0.76	**0.94**	0.75	0.76
1	0.91	**0.98**	0.97	0.97	0.96	0.97	0.97
2.5	**0.99**	0.89	0.92	0.92	0.92	**0.99**	**0.99**

low excursion situations, and the PGS normalization or the CoI method in cases with higher phase excursions. In almost every situation, the ISS method outperforms the other phase recovery methods at the cost of more time consuming calculations. It is worth to note that the simplest PGLS normalization gives high performance even in the cases where there are inhomogeneities in both beams.

C. Other tests

In this subsection we present different tests to describe the behavior of the methods with respect to three configuration parameters. We start by analyzing the performance of the ISS phase recovery method at different smoothness values of the phase solution. Afterwards, we test the performance of the CoI, arccos and ISS methods when the optical setup is modified in order to change the mean speckle size and the reference to object beam intensity ratio.

C.1. ISS smoothness parameter

The configuration of the smoothness parameter in the ISS method requires a special consideration in order to achieve the best performance of the phase recovery method. The simulated cases presented in the previous subsections were performed with different p setting and the results for the homogeneous illumination situation are shown in Fig. 3. For the sake of clarity, the PGS and PGLS data were plotted with the same line because they give very similar SSIM results. The SBI normalization method gave the best result and noise robustness for the lowest excursion phase field. Nevertheless, the PGS and PGLS normalization methods gave a performance similar to the SBI technique when $p < 10^{-3}$ for the high SNR case. In every other cases with higher phase excursion, the PGS and PGLS methods outperformed the SBI normalization almost independently of p, being $p = 1$ a reasonable choice. We note that the PGLS method gave a performance quite similar to PGS at a reduced computation cost.

C.2. Mean speckle size

Similar simulations were performed in order to analyze the behavior of the CoI, arccos-SBI, ISS-SBI ($p = 10^{-4}$) and ISS-PGLS ($p = 10^{-4}$ and $p = 1$) methods in order to analyze the mean speckle size by modifying the optical setup. We used $SNR = 15$

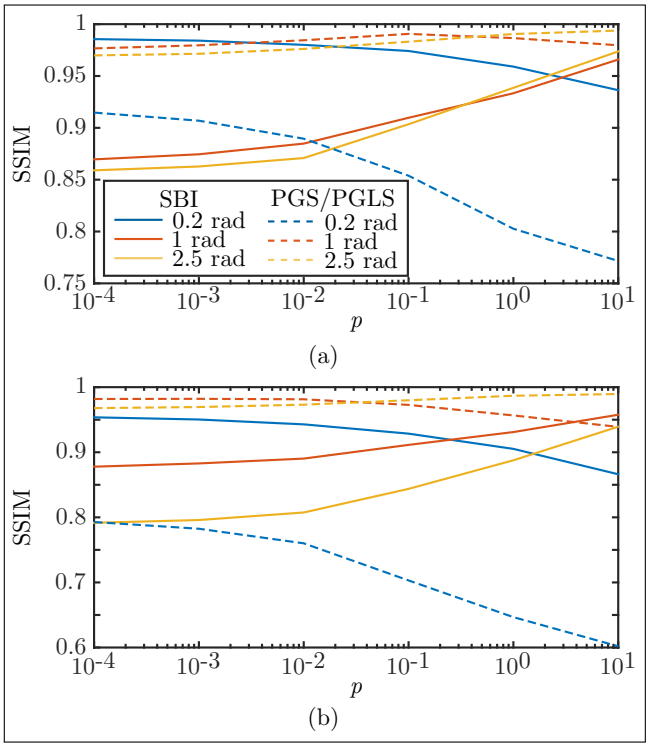

Fig. 3. Smoothness parameter (p) sweep for the ISS method in homogeneous illumination. Solid lines correspond to SBI normalization and dashed lines to the PGS and PGLS techniques. SSIM results for three phase excursion situations. (a) SNR = 18 dB , (b) SNR = 10 dB.

dB, $L = 25$ and homogeneous illumination. The obtained SSIM indices are shown in Fig. 4 for the following situations: (solid lines) $A_\phi = 0.2$ rad and (dashed lines) $A_\phi = 1.5$ rad. The CoI method was implemented with and without the approximation of considering as unity the term depending on the modulation intensities in Eq. 6. We did not detect any appreciable difference between the SSIM indices obtained by both versions of the CoI method. From Fig. 4, the main observation is that every method gave better results for low sized speckle grain. In the case of higher phase excursion, the phase recovery performance can be severely impoverished by the use of $s > 1.5$ px. In the low phase excursion case, the SBI normalization method provided a framework considerably robust to changes in the mean speckle size.

C.3. Reference to object beam intensity ratio

We used different simulated images to study the performance of the methods with respect to the relation r of mean intensities between the reference and the object beams $r = I_R / \bar{I}_O$. We fixed a constant noise variance σ_G^2 corresponding to the condition of SNR = 10 dB at $r = 2$. The simulated intensity values were digitized to 8-bit gray levels. Fig. 5 shows the SSIM indices obtained for these simulations when the CoI, arccos-SBI, ISS-SBI ($p = 10^{-4}$) and ISS-PGLS ($p = 10^{-4}$ and $p = 1$) phase recovery methods were applied. In general, the range $2 \leq r \leq 6$ is recommended for the application of these methods. It is worth noting the invariance of the phase recovery performance with respect to r achieved by using the SBI normalization in low phase excursion cases. Also, this kind of invariance is observed in the CoI and the ISS-PGLS results (with the CoI seed solution) when

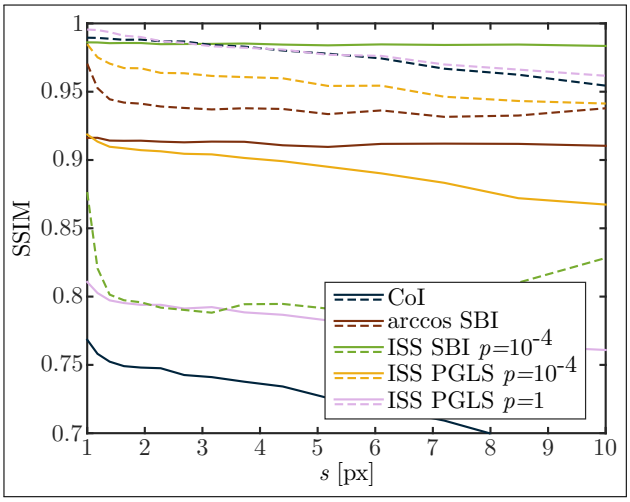

Fig. 4. SSIM indices given by the CoI, arccos SBI and ISS PGLS methods in a simulation sweep of s with homogeneous illumination and $SNR = 15$ dB. Solid lines correspond to $A_\phi = 0.2$ rad and dashed lines to $A_\phi = 1.5$ rad.

$r > 4$ for the ISS-PGLS method and also in the CoI techniaque in the high phase excursion situation.

4. EXPERIMENTAL RESULTS

We used a Twyman-Green based interferometer with a 532 nm laser to observe the out-of-plane displacement field at the surface of the metal electrode of a piezoelectric disk transducer (PZT disk). As described in Ref. [33], this setup was used to acquire a sequence of images that contained information about the temporal evolution of the sample and a nonlinear decomposition framework allowed to recover the phase field evolution. In this work, we took advantage of the whole sequence by using the temporal mean value of intensity $\bar{I}_t$ instead of I_i for the PGLS normalization procedure. However, only two images

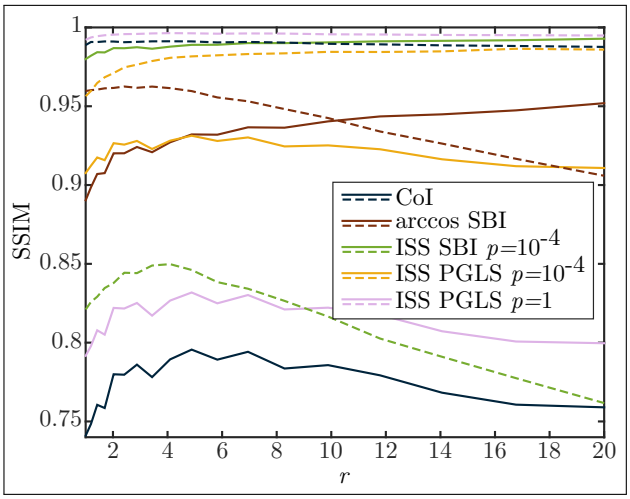

Fig. 5. SSIM indices given by the CoI, arccos SBI and ISS PGLS methods in a simulation sweep of the intensity ratio r with homogeneous illumination and $SNR = 10$ dB at $r = 2$. Solid lines correspond to $A_\phi = 0.2$ rad and dashed lines to $A_\phi = 1.5$ rad.

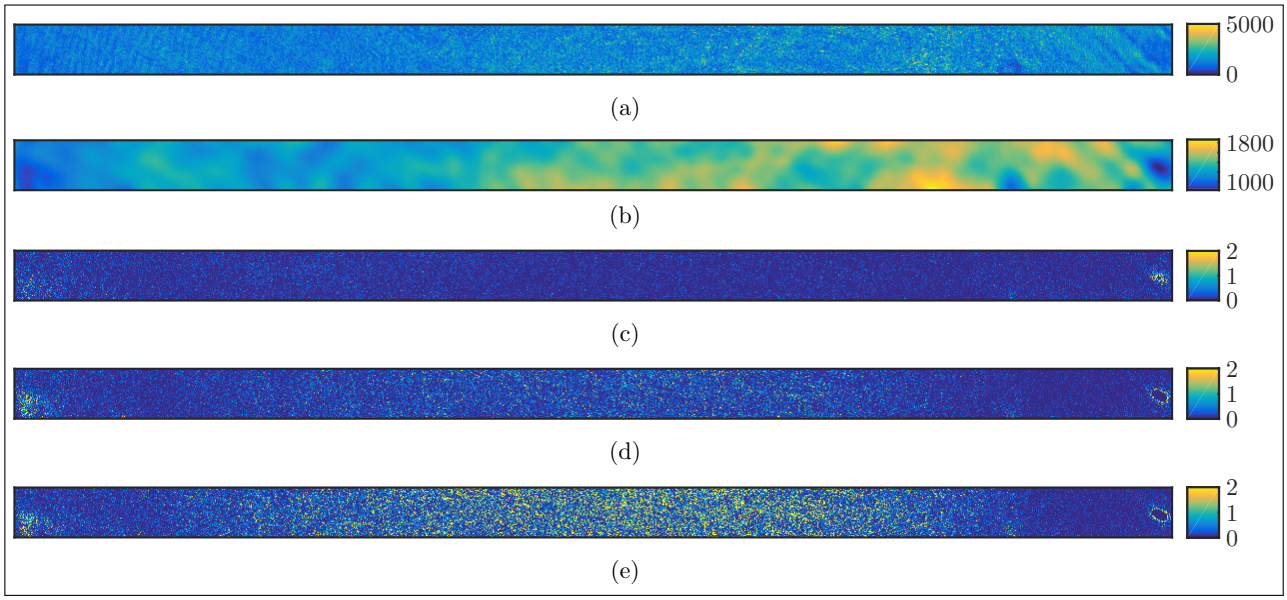

Fig. 6. (a) Speckle interferogram recorded at the initial state. (b) Temporal mean value of the intensity $\bar{I}_t$ used for the PGLS normalization. Normalized DSPI-FP at (c) ΔV_1, (d) ΔV_2 and (e) ΔV_3.

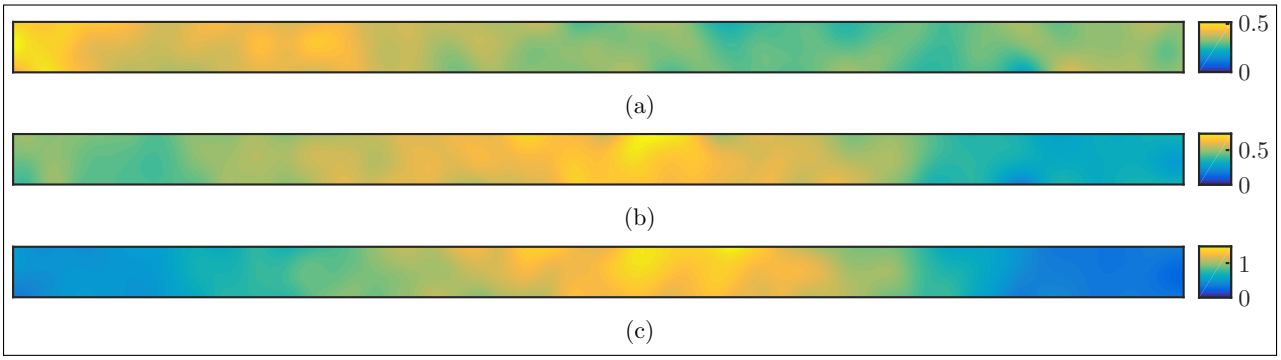

Fig. 7. Phase map recovered by the ISS-PGLS method at (a) ΔV_1, (b) ΔV_2 and (c) ΔV_3.

of the PZT disk were used to measure the displacement field between an initial state for a given applied voltage V_i and a second deformed state when the applied voltage was varied to $V_d = V_i + \Delta V$. In Fig. 6(a) we show the speckle interferogram recorded at the initial state, which was acquired for a reduced stripe form region of interest which included the center and two opposing borders of the PZT disk. The temporal mean value of intensity $\bar{I}_t$ displayed in Fig. 6(b) presents a typical uneven illumination situation. Figs. 6(c-e) show the normalized DSPI-FP for three different ascending ΔV values.

The object phase fields given by the ISS-PGLS method are presented in Fig. 7 for the three considered ΔV. Fig. 8 allows to compare the smoothness and the accuracy of the different solutions given by the CoI, arccos and ISS methods with the PGLS normalization in each of the three ΔV studied cases. It is seen that in the case of ΔV_1, the amplitude of displacement was not sufficient to be recovered and discriminated from noise by any method. In higher excursion cases, the CoI method gave phase distributions with higher values than other techniques because the local variations of the illumination and the noise acquired within the $L \times L$ windows caused a reduction of correlation and therefore, an increase in the recovered phase (see Eq. (7)). On the other hand, the arccos method based in a median filtering process gave lower values for the phase map than the other two techniques. The phase values recovered by the ISS method are midway between the arccos and the CoI results and also show improved smoothness.

5. CONCLUSIONS

This work provides an analysis that serves as a guidance to take full advantage of the sensibility of the DSPI technique, which is especially suitable for the inspection of microsystems with nanometrical displacement fields. The fringeless speckle interferograms obtained in these cases require especific normalization and phase recovery approaches. In this work we describe and compare three different methods of phase recovery in DSPI with fringeless patterns. We emphasize the necessity of a robust normalization method for the arccos and ISS phase recovery methods and provide three approaches, where two of them do not require the acquisition of new images or the modification of the optical setup and estimate the modulation intensity from the available interferograms instead. As the CoI method does not require a normalized DSPI-FP, it was used as a starting point providing an initial phase guess solution for the normalization process. We used simulated DSPI interferograms

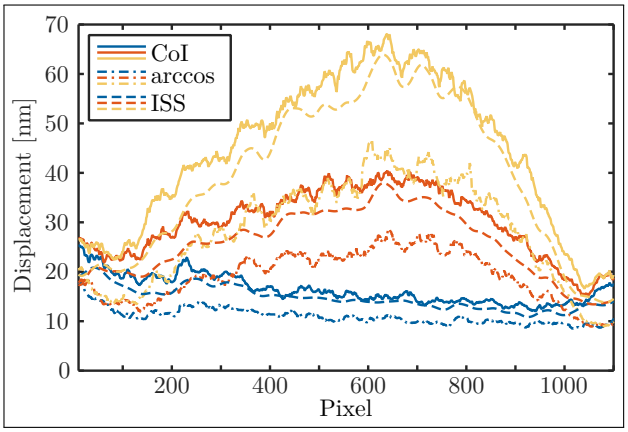

Fig. 8. Values at the central row in the phase maps recovered by the CoI, arccos and ISS methods for different ΔV.

to perform an analysis of the behavior of all methods depending on the SNR, the phase excursion, the illumination condition, the reference to object beam intensity ratio and the mean speckle size. The best performance, robustness and versatility was given by the ISS method at the cost of higher computational complexity. The observed behavior for the ISS method with respect to variations in the smoothness parameter and the phase excursion suggested, as mentioned in Ref. [10], that weighted errors or spatially varying smoothness parameter (see [34]) could improve the performance in the extraction of phase maps with noticeable spatial variability of the phase excursion. On the other hand, a simple filtering and arccosine based procedure proved to be sufficient in almost every situation to obtain a rapid inspection of the underlying phase map corresponding to the displacement field in the sample. The CoI method provides, not only a necessary initial phase guess to other methods, but also the best solution in cases presenting higher phase excursions. Regarding the normalization methods, the SBI technique is recommended for low phase excursion situations and the PGLS approach for higher phase excursions. Finally, we have also tested the application of the proposed methods for the measurement of nanometric displacements over the surface of a piezoelectric transducer. The proposed methods behaved in accordance with the results previously obtained in the numerical analysis and a minimum displacement field with range $d \in [15, 40]$ nm was similarly observed by using the CoI and the ISS methods.

REFERENCES

1. W. Osten, *Optical inspection of Microsystems* (CRC Press, 2007).
2. A. Asundi, *Digital holography for MEMS and microsystem metrology*, vol. 7 (John Wiley & Sons, 2011).
3. R. S. Sirohi, *Introduction to Optical Metrology* (CRC Press, 2015).
4. M. Kujawińska, M. Józwik, and A. Styk, "Parallel multifunctional system for mems/moems and microoptics testing," Handbook of Optical Dimensional Metrology p. 451 (2016).
5. F. Amiot, "Full-field measurements for the mechanics of micrometer-sized structures," Ph.D. thesis, ENS Cachan (2015).
6. G. H. Kaufmann, *Advances in speckle metrology and related techniques* (John Wiley & Sons, 2011).
7. P. K. Rastogi, "Digital speckle pattern interferometry and related techniques," Digital Speckle Pattern Interferometry and Related Techniques, by PK Rastogi (Editor), pp. 384. ISBN 0-471-49052-0. Wiley-VCH, December 2000. **1** (2000).
8. B. Bhaduri, M. Kothiyal, and N. K. Mohan, "A comparative study of phase-shifting algorithms in digital speckle pattern interferometry," Optik-International Journal for Light and Electron Optics **119**, 147–152 (2008).
9. Z. Malacara and M. Servin, *Interferogram analysis for optical testing*, vol. 84 (CRC press, 2005).
10. M. Wielgus, K. Patorski, P. Etchepareborda, and A. Federico, "Continuous phase estimation from noisy fringe patterns based on the implicit smoothing splines," Opt. Express **22**, 10775–10791 (2014).
11. J. H. Galeti, R. T. Higuti, E. C. Silva, and C. Kitano, "Nanodisplacement measurements of piezoelectric flextensional actuators using a new interferometry homodyne method," IEEE Transactions on Instrumentation and Measurement **64**, 1256–1265 (2015).
12. M. Takeda, H. Ina, and S. Kobayashi, "Fourier-transform method of fringe-pattern analysis for computer-based topography and interferometry," J. Opt. Soc. Am. **72**, 156–160 (1982).
13. K. Qian, "Windowed fourier transform method for demodulation of carrier fringes," Opt. Eng. **43**, 1472–1473 (2004).
14. C. Quan, C. J. Tay, F. Yang, and X. He, "Phase extraction from a single fringe pattern based on guidance of an extreme map," Appl. Opt. **44**, 4814–4821 (2005).
15. A. Federico and G. H. Kaufmann, "Phase retrieval in electronic speckle pattern interferometry using the continuous wavelet transform," in "IV Iberoamerican Meeting of Optics and the VII Latin American Meeting of Optics, Lasers and Their Applications," (International Society for Optics and Photonics, 2001), pp. 162–165.
16. P. Etchepareborda, A. L. Vadnjal, A. Federico, and G. H. Kaufmann, "Phase-recovery improvement using analytic wavelet transform analysis of a noisy interferogram cepstrum," Opt. Lett. **37**, 3843–3845 (2012).
17. V. Madjarova, H. Kadono, and S. Toyooka, "Dynamic electronic speckle pattern interferometry (despi) phase analyses with temporal hilbert transform," Opt. Express **11**, 617–623 (2003).
18. M. Servin, J. A. Quiroga, and M. Padilla, *Fringe pattern analysis for optical metrology: theory, algorithms, and applications* (John Wiley & Sons, 2014).
19. R. Kulkarni and P. Rastogi, "Simultaneous estimation of unwrapped phase and phase derivative from a closed fringe pattern," Optics and Lasers in Engineering (2016).
20. M. B. Bernini, A. Federico, and G. H. Kaufmann, "Normalization of fringe patterns using the bidimensional empirical mode decomposition and the hilbert transform," Appl. Opt. **48**, 6862–6869 (2009).
21. M. Trusiak, M. Wielgus, and K. Patorski, "Advanced processing of optical fringe patterns by automated selective reconstruction and enhanced fast empirical mode decomposition," Opt. Laser. Eng. **52**, 230–240 (2014).
22. D. R. Schmitt and R. Hunt, "Optimization of fringe pattern calculation with direct correlations in speckle interferometry," Applied optics **36**, 8848–8857 (1997).
23. L. P. Tendela, G. E. Galizzi, A. Federico, and G. H. Kaufmann, "A fast method for measuring nanometric displacements by correlating speckle interferograms," Optics and Lasers in Engineering **50**, 170–175 (2012).
24. J. W. Goodman, *Speckle phenomena in optics: theory and applications* (Roberts and Company Publishers, 2007).
25. X. Yang, Q. Yu, and S. Fu, "Determination of skeleton and sign map for phase obtaining from a single espi image," Opt. Comm. **282**, 2301–2306 (2009).
26. S. Mirza, R. Kumar, and C. Shakher, "Study of various preprocessing schemes and wavelet filters for speckle noise reduction in digital speckle pattern interferometric fringes," Optical Engineering **44**, 045603–045603–6 (2005).
27. L. P. Tendela, G. E. Galizzi, A. Federico, and G. H. Kaufmann, "Measurement of nanometric displacements by correlating two speckle interferograms," Appl. Opt. **50**, 1758–1764 (2011).
28. W. Xu, C. Chang, Y. S. Hung, S. Kwan, and P. C. W. Fung, "Order statistics correlation coefficient as a novel association measurement with applications to biosignal analysis," IEEE Transactions on Signal Processing **55**, 5552–5563 (2007).
29. C. De Boor, "A practical guide to splines (revised ed.)," New York

(2001).
30. P. Rabinowitz, *Numerical methods for nonlinear algebraic equations* (1988).
31. G. H. Kaufmann, “Phase measurement in temporal speckle pattern interferometry using the fourier transform method with and without a temporal carrier,” Opt. Comm. **217**, 141–149 (2003).
32. Z. Wang, A. Bovik, H. Sheikh, and E. Simoncelli, “Image quality assessment: from error visibility to structural similarity,” IEEE Trans. on Image Proc. **13**, 600–612 (2004).
33. P. Etchepareborda, A. Bianchetti, F. E. Veiras, A. L. Vadnjal, A. Federico, and G. H. Kaufmann, “Comparison of real-time phase-reconstruction methods in temporal speckle-pattern interferometry,” Appl. Opt. **54**, 7663–7672 (2015).
34. A. Federico and G. H. Kaufmann, “Application of weighted smoothing splines to the local denoising of digital speckle pattern interferometry fringes,” in “Fringe 2005,” (Springer, 2006), pp. 208–211.